

# The consequences of the mechanical environment of peripheral arteries for nitinol stenting

Michael Early · Daniel J. Kelly

Received: 3 November 2010 / Accepted: 30 July 2011 / Published online: 11 August 2011  
© International Federation for Medical and Biological Engineering 2011

**Abstract** The use of stents in peripheral arteries has not been as successful as in coronary arteries, with high rates of restenosis and stent fracture common. Normal joint flexion induces a range of forces on the arteries, which has an unknown effect on the outcomes of stenting. The objective of this study is to determine how physiological levels of vessel bending and compression following stent implantation will influence the magnitude of stent stresses and hence the risks of fatigue fracture. A further objective is to compare how this mechanical environment will influence arterial stresses following implantation of either stainless steel or nitinol stents. To this end, models of both nitinol and stainless steel stents deployed in peripheral arteries were created, with appropriate loading conditions applied. At high levels of bending and compression, the strain amplitude threshold value for fatigue failure is exceeded for nitinol stents. Bending was predicted to induce high stresses in the artery following stenting, with higher arterial stresses predicted following implantation of a stainless steel stent compared to a nitinol stent. Both bending and compression may contribute to stent fracture by increasing the strain amplitude within the stent, with the dominant factor dependant on location within the arterial tree. For the specific stent types investigated in this study, the model predictions suggest that compression is the dominant mechanical factor in terms of stent fatigue in the femoral arteries, whereas bending is the most significant factor in the popliteal artery. To increase fatigue life and reduce arterial injury, location specific stent designs are required for peripheral arteries.

**Keywords** Peripheral arteries · Nitinol stents · Bending · Compression · Finite element analysis

## 1 Introduction

Stenting in peripheral arteries has proved problematic, with success rates hindered by in-stent restenosis and stent fracture. The femoral and popliteal arteries are particularly problematic in this regard. Initially, balloon-expanded stainless steel stents were used, but the high initial technical success rates diminished over time, until the cumulative patency rates were the same for angioplasty alone and stenting after 1 and 2 years [6]. The problems associated with the procedure lead to the development of more flexible shape-memory alloy (usually nitinol) stents. While these newer stents decreased the rates of restenosis compared with angioplasty alone [29], restenosis rates are still higher than in coronary arteries. Furthermore, the advent of drug-eluting stents has not shown the improvements in peripheral arteries [8, 9] that have been demonstrated in coronary arteries [19].

There are many differences between coronary and peripheral arteries that may be responsible for these findings. It has been suggested that differences in stent and artery geometry and material properties do not lead to higher levels of arterial injury that might explain the higher rates of restenosis in peripheral arteries [10]. Furthermore, the pulsatile cardiac cycle is not predicted to cause stent fatigue failure. The mechanical environment of the peripheral arteries, caused by joint flexion, may be contributing to the higher rates of restenosis in these arteries. The forces acting on the superficial femoral artery have been identified as axial, torsional, compressive and flexional [17]. The effect of these forces has been quantified in angiographic studies [7, 23, 31], which has motivated the development to in vitro mock artery

---

M. Early · D. J. Kelly (✉)  
Trinity Centre for Bioengineering, School of Engineering,  
Trinity College, Dublin, Ireland  
e-mail: kellyd9@tcd.ie

models to better understand how the bending and compression experienced by peripheral vessels influences the outcomes of stenting [23]. Bending and compression were shown to cause fatigue fracture in stents, with the fracture rate strongly dependant on the stent design. As a correlation exists between stent fracture and rates of restenosis [27], predicting fatigue related stent fracture for new designs is critically important.

Finite element analysis has been a commonly used tool for analysing aspects of the stent–artery interaction [2–5, 13, 14, 18, 20–22, 25, 26, 28, 34, 36]. Most of the published studies investigate balloon-expanded stainless steel stents in coronary arteries. While the interaction of nitinol stents with a carotid artery [35] and the bending of a renal stent without considering the stent–artery interaction have been studied [16], most studies do not consider how vessel deformation will influence stent–artery interactions. We have previously demonstrated that vessel bending significantly influences arterial stresses and the risk of stent fatigue failure following the implantation of a balloon expandable stent (BES) [11]. In that study, models of peripheral arteries were created that considered the non-linear, inhomogeneous mechanical properties of these tissues, into which BES were expanded. The model predicted that bending of a stented vessel could induce comparable levels of arterial stresses to that induced during balloon expansion of a BES. What remains unclear is how the more flexible nitinol self-expanding stents (SES) that are now more commonly used in peripheral arteries will respond to this complex mechanical environment, both in terms of arterial injury and the stresses developed within the stent itself that may lead to fatigue failure. The aim of this study is therefore to investigate how the mechanical environment of the lower limb influences the biomechanics of SES. Our hypothesis is that vessel bending caused by joint flexion induces (i) elevated stress levels in the stented artery which could lead to increased vessel injury and (ii) an environment which is likely to cause stent fatigue failure for both nitinol SES and stainless steel BES. This hypothesis will be tested by simulating the deployment of SES and BES in peripheral arteries and applying bending and compressive boundary conditions to the artery. The study will also consider how simple changes in SES design influence arterial stresses and the risk of stent fatigue failure. Specifically this study will investigate the influence of SES strut thickness, which is perhaps one of the simplest design change options available that can influence both the flexibility and radial strength of a stent.

## 2 Methods

The Finite element method was used to simulate the deployment of BES and SES in a peripheral artery and

subsequent bending of that artery (Marc/Mentat 2007, MSC software corporation, Santa Ana, CA, USA). All models used an implicit single-step Houbolt solver. Discrete contact was implemented in all cases, with the coefficient of friction assumed to be zero. Large strain analysis with an updated Lagrangian procedure was used. Marc type 7 elements were used for the stents, and type 84 elements with Hermann integration were used to mesh the arteries.

The artery was modelled as a hollow cylinder with an inner diameter of 8 mm, a thickness of 1 mm and a length of 40 mm. The diameter of 8 mm represented an average vessel diameter between the iliac and the superficial femoral artery. This was sub-divided into three concentric layers representing the intima, media and adventitia of the vessel in the ratio 15:54:31 [30]. A plaque was not included, as this creates several other variables (plaque material properties, thickness, and eccentricity). More generalised studies which do not look at patient specific geometries sometimes omit the plaque when comparing stent designs [3]. The BES was based on a Palmaz slotted tube (Fig. 1a), closed cell design that had a length of 20 mm, a thickness of 150  $\mu\text{m}$  and an initial diameter of 3 mm (Fig. 1a). The SES was a generic stent design roughly based on commercially available designs such as the Smart stent (Cordis Corporation, NJ), see Fig. 1b. It had a length of 20 mm, an initial diameter of 10 mm and a strut thickness of 150  $\mu\text{m}$ . Stent design was studied by creating similar stents with strut thickness of 100 and 250  $\mu\text{m}$ .

A bi-linear material model with plasticity was used to represent material properties based on micro-samples for the stainless steel stents. Nitinol was described using a material model available in MSC/Marc software based on the model presented by [1] which is suitable for temperature- and stress-dependent phase transformations. The constants were taken from [12] and have been used elsewhere in the literature [35]. The non-linear behaviour of the arteries was described using third-order Mooney-Rivlin constitutive strain energy functions. Constants were

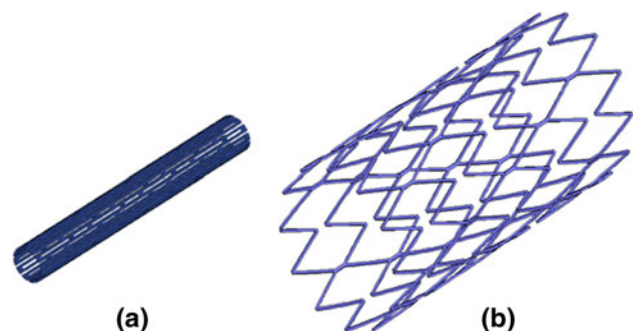


**Fig. 1** Geometry of **a** balloon expandable stent in unexpanded configuration and **b** self-expanding stent at initial configuration

obtained for the three layers of the human iliac artery [15], further details of which are available elsewhere [10]. This material model assumes isotropy of the vessel wall, which is a simplification of the actual behaviour.

Appropriate boundary conditions were used to simulate physiological loading of the artery, stent expansion, and bending and compression of the artery following stent expansion. Symmetrical boundary conditions were applied to all nodes which coincided with the symmetrical planes. An average blood pressure of 13.3 kPa was applied to the internal faces of the artery wall. An axial stretch of 1.07 [30] was then applied to one end of the artery.

The BESs and SESs had different modes of expansion. The BESs were expanded by applying a linearly increasing pressure directly to the internal faces of the stent. This predicted a non-uniform stent expansion. To achieve a uniform final shape, the stent was constrained using springs which had a variable stiffness which was a function of the local stent diameter [11]. These springs had a low stiffness until the stent reached a specified diameter, at which point the stiffness increased, preventing further stent expansion (i.e. mimicking a low compliance angioplasty balloon). BESs were expanded to a pre-recoil diameter of 10 mm, representing an expansion ratio of 1.25, typical of that used in vivo. Removing the pressure allows the stent to recoil.

SESs are initially in the fully expanded, stress free configuration and are compressed into a sheath to fit into the artery. Once in place, the sheath is withdrawn and the stent elastically attempts to return to its original shape, until the artery prevents further expansion. This process can be simulated by beginning with the stent fully expanded and unstressed. Artery elements, which are coincident with the stent at the start, are deactivated, see Fig. 2a. The stent is compressed using a rigid sheath (b) until it is sufficiently crimped to fit inside the artery (c). The artery elements are then reactivated, and the physiological

loading is applied to the artery (d). Laterally withdrawing the sheath (e) allows the stent to expand (f). Because the stent expands from one end to the other, this process is not symmetrical longitudinally. However, analysis of a full stent showed that the difference in assuming symmetry in terms of arterial stresses was very small. In order to reduce the considerably computational costs, symmetrical boundary conditions were applied to the SES models.

Bending was simulated by rotating the end of the artery. The end of the artery was rotated by 60° (see Fig. 3a), with analysis undertaken every 6°. The centre of rotation was coincident with the centre of the artery. Compression was simulated in the same manner by moving the end of the artery axially through a maximum of 25% of the pre-stretched artery length.

As elevated arterial stresses are hypothesised to lead to greater injury and thus restenosis, and stent fracture is an important determinant of stenting success, an analysis of the arterial von Mises stresses and the stent fatigue properties was undertaken. The von Mises stress was chosen as a simple predictor of tissue failure and hence the likelihood of vessel injury, though arguments could be made for using other stress measures (e.g. the first principal stress). The average value of the integration points within each element was taken to give a single value for each element, and the volumes of arterial tissue within designated stress ranges were plotted. Arterial stress distributions following bending were analysed at 0° (following recoil), 12°, 18°, 36° and 54°. The values of 12° and 18° represent close to average bending values of the distal SFA/proximal popliteal artery at knee/hip flexions of 70°/20° and 90°/90° of  $11^\circ \pm 12^\circ$  and  $15^\circ \pm 14^\circ$ . Likewise, the values of 36° and 54° represent the popliteal artery at knee/hip flexions of 70°/20° and 90°/90° of  $33^\circ \pm 21^\circ$  and  $54^\circ \pm 25^\circ$  [23]. Arterial stresses following compression are not presented. This is because artery buckling, which depends on the

**Fig. 2** Deployment of self-expanding stent. After **a** initial configuration, **b** artery elements are deactivated and **c** sheath is used to crimp stent. This allows **d** artery elements to be reactivated, and **e** the stent to be withdrawn allowing **f** full stent expansion

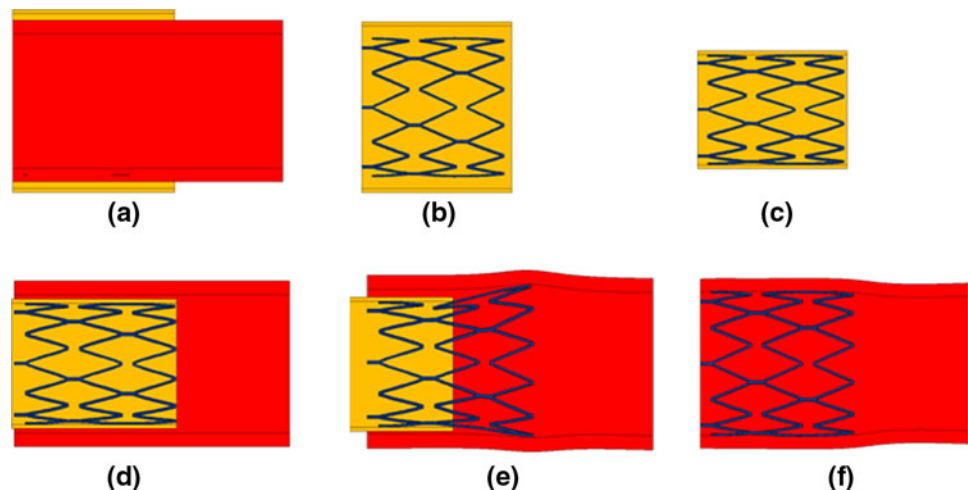
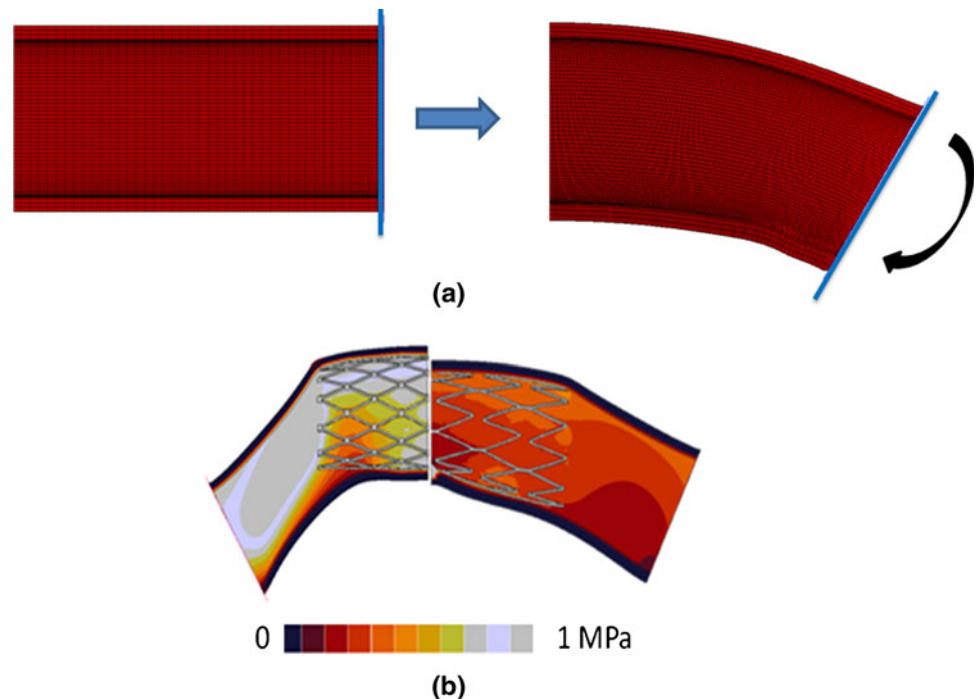


**Fig. 3** **a** Application of bending boundary condition. **b** Contour plots of BES (left) and SES (right) following 30° of bending



arbitrary length of the unstented artery segment, dictates the arterial stresses. The influence of compression on stent deformation is considered.

For stainless steel, the stress amplitude ( $\sigma_a$ ) and the mean stress ( $\sigma_m$ ) were plotted on a Goodman curve for each integration point of the stent elements. Using a fatigue endurance limit ( $S_e$ ) of 420 MPa and an ultimate tensile strength ( $S_{ult}$ ) of 600 MPa [33], a factor of safety could be determined for each integration point and represented graphically (Eq. 1). For nitinol SES, the strain amplitude was measured. A threshold value of 0.4% [24] was taken, with a *FOS* calculated by comparing the maximum strain amplitude ( $SA_{max}$ ) to this value (Eq. 2).

$$\frac{1}{FOS_{steel}} = \frac{\sigma_m}{S_{ult}} + \frac{\sigma_a}{S_e} \quad (1)$$

$$\frac{1}{FOS_{nitinol}} = \frac{0.4}{SA_{max}} \quad (2)$$

### 3 Results

#### 3.1 Balloon-expanded stent

In each layer of the artery, bending the artery following deployment of a BES increases the amount of the tissue at higher stresses, see Fig. 4. For example, applying 12° of bending places 46.1% of the intima at stresses between 500 and 750 kPa, compared to 1.5% following recoil of the stent (0° of bending). As the amount of bending is increased, the amount of tissue in the higher stress ranges

(500 kPa or greater) increases. Similar patterns of stress increases are predicted in the media and adventitia, but the range of stresses in these layers is an order of magnitude lower. The peak stresses are located at the end(s) of the stent, where the artery is in tension, as shown in Fig. 3b. As the bending is increased, high stresses are also predicted proximally and distally to the stent, though the location of the peak stresses is the same.

As well as increasing the arterial stresses, bending the artery induces a strain environment in the stent which, while not predicting fatigue fracture, lowers the *FOS* from 1.43 at 6° to 1.14 at 60°, see Fig. 5e. Plotting each integration point on a Goodman curve shows that as well as the factor of safety decreasing with increasing bending, the amount of points close to the pass/fail line ( $FOS = 1$ ) increases substantially (Fig. 5a–d). The stent does not recover to its original expanded diameter on unbending of the artery (for any amount of initial arterial bending).

#### 3.2 Self-expanding stents

##### 3.2.1 Bending

Bending an artery following implantation of a SES is predicted to increase the stresses in all three layers of the artery, as shown in Fig. 6. Small amounts of bending (12° and 18°) causes only minor changes in the arterial stress states. A greater effect is seen when the bending is increased to 36° and 54°. After 54° of bending, 20.8% of the intima is at stresses between 500 and 750 kPa, with a

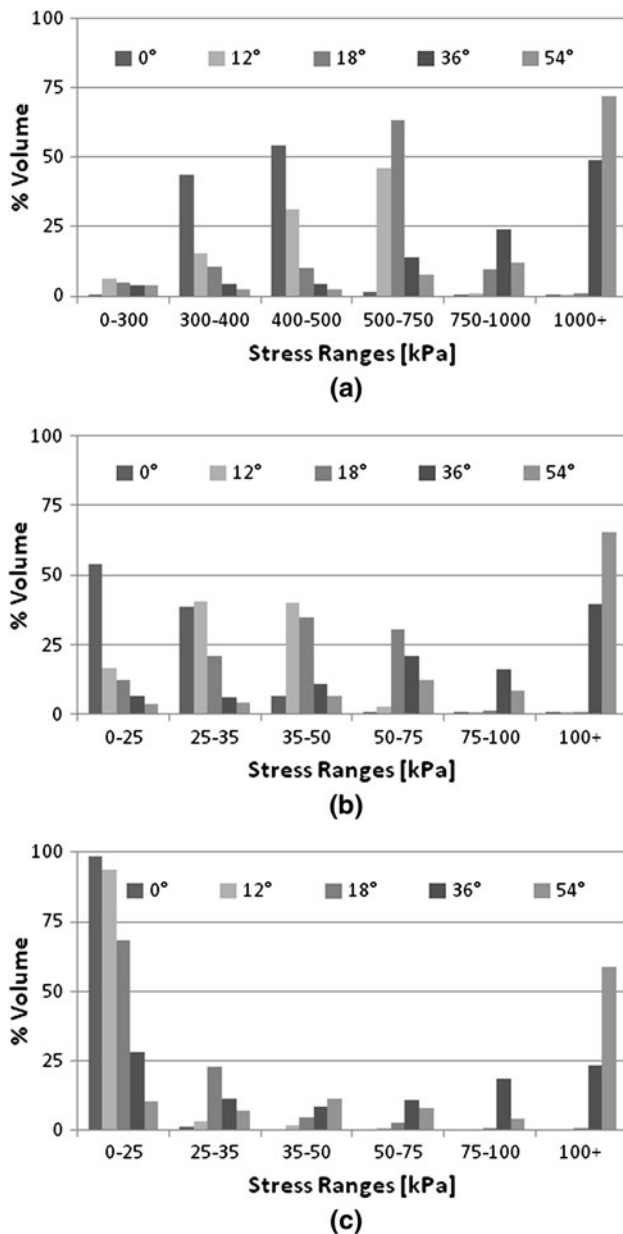


**Fig. 4** Stress distributions in **a** intima, **b** media and **c** adventitia at various stages of bending following insertion of BES

further 10.2% at stresses of 750 kPa or greater. Similar trends are seen in the media and adventitia, where bending of 12° and 18° made small changes to the stress distributions, while bending of 36° and 54° placed more of the tissue at higher stress ranges. The peak stresses are in the same areas as with a BES, Fig. 3b, although the magnitudes of peak stresses are lower.

The maximum strain amplitude in the stent also increases, with a corresponding reduction in the FOS, as bending is applied (Fig. 7a). Up to high levels of bending (54°), the maximum strain amplitude is not predicted to be higher than the threshold value of 0.4%, and so fatigue

failure is predicted not to occur. However, at 60° of bending, a maximum strain amplitude value of 0.57% is reached.

### 3.2.2 Compression

Small amounts of artery compression induce relatively high strain amplitude values in SESs, which gradually increases with compression (Fig. 7b). Between 15 and 17.5% compression is predicted to cause the SES to exceed the strain amplitude threshold value for fatigue failure.

### 3.2.3 Stent design

Varying the strut thickness is predicted to alter the stresses in each arterial layer at the various degrees of bending (Fig. 8). The trends are similar for each strut thickness, with more significant differences in the stress states predicted after bending of 36° and 54°. Using a thinner strut (100 μm) reduces the amount of intimal tissue at higher stresses. After 54° of bending, the amount of the intima between 500 and 750 kPa is reduced from 22.3% for 250 μm thick struts to 20.8% for 150 μm thick struts and 15.5% for 100 μm thick struts. In the media and adventitia, the same trends are observed, where implanting a stent with thicker struts is predicted to increase the amount of tissue at higher stresses. For all values of bending, each of the SES models is predicted to produce lower arterial stresses than the BES model.

SES strut thickness also affected the predicted maximum stent strain amplitude following bending (Fig. 7a). Increasing the strut thickness from 100 to 250 μm was predicted to reduce the maximum strain amplitude after any amount of bending, with the highest values (after 60° of bending) being reduced from 0.66 to 0.39. The 100 μm strut stent exceeds the 0.4% threshold value after 30° of bending, while this threshold is only exceeded after 60° of bending when the strut thickness is 150 μm. The maximum strain amplitude value predicted in the stent with the thickest struts (250 μm) is 0.39%, marginally lower than the value of 0.4% required for fatigue failure.

In comparison, increasing the strut thickness is generally predicted to result in a greater strain amplitude in the stent following arterial compression, as shown in Fig. 7b. The exception to this is seen at higher levels of compression (>15%), where the 250 μm stent has a lower strain amplitude than the 150 μm stent.

## 4 Discussion

The results presented in this study provide further evidence to suggest that stainless steel stents similar in design to that



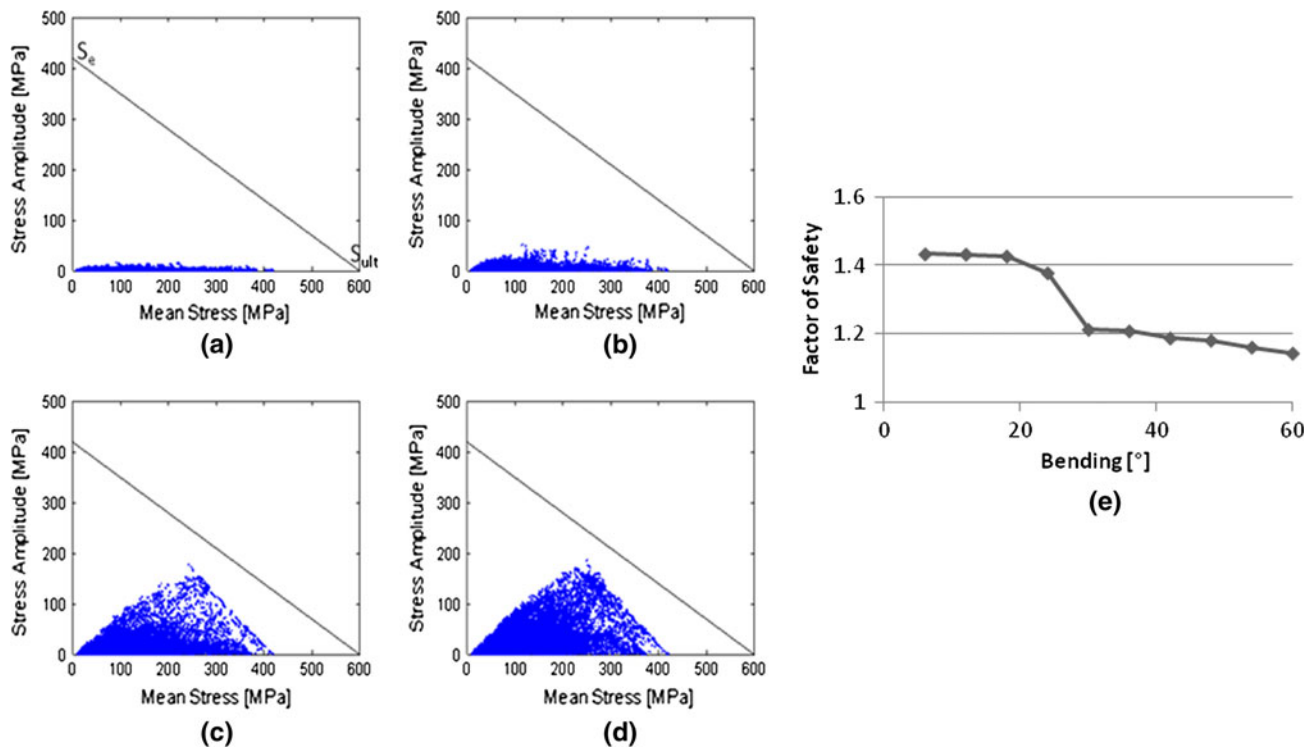


**Fig. 5** Goodman diagram for BES after **a** 12°, **b** 18°, **c** 36° and **d** 54° of bending and **e** minimum FOS for BES at various stages of bending

investigated here may be incompatible with arteries subjected to bending [11]. Such stents, stiffer than the arteries into which they are implanted owing to the stent geometry and material properties, cause significant increases in stress in all three layers of the artery. The high peak stresses predicted in the artery and the volume of tissue within high stress ranges could lead to extensive tissue damage, and hence may play a role in determining subsequent neointimal hyperplasia. Furthermore, bending the artery causes permanent deformation of the stent, which may negatively affect the dynamics of blood flow in the vessel, which can also contribute to restenosis. These factors may help explain the lack of improvement with this type of stenting relative to PTA alone in femoral arteries [6]. Although the bending cycle simulated here is not predicted to cause fatigue failure of the stent (FOS greater than one for all integration points), this is for an idealised artery and a relatively short stent. A calcified or eccentric plaque [32], a longer lesion (and stent) or a more irregular vessel geometry would be amongst the factors that could reduce the factor of safety and lead to stent fatigue fracture.

The higher flexibility offered by shape-memory alloy stents was predicted to reduce the arterial stresses following bending. This suggests that damage to the arterial tissue is reduced, and restenosis rates might be expected to be lower in arteries where a SES is used compared with a traditional BES like that investigated in this study. Clinical

studies have shown that, unlike steel stents, the use of nitinol stents in the femoral artery improves rates of restenosis compared with balloon angioplasty alone [29].

The fracture of nitinol stents continues to hinder their use in peripheral arteries, particularly in the SFA and popliteal artery. One approach to determining the factor of safety for a nitinol stent is to use the finite element method to predict the strain amplitude within the stent. A strain amplitude threshold value of 0.4% has been determined experimentally to cause fatigue failure after 10 million pulsatile cycles [24]. The FE methodology presented in this study can be used to predict the likelihood of fatigue failure for any given stent design. Both bending and compression may contribute to stent fracture by increasing the strain amplitude, with the dominant factor dependant on location (Table 1). For example, in the femoral and femoro-popliteal arteries, the results of the study suggest that compression is the dominant mechanical factor in terms of stent fatigue, whereas in the popliteal artery bending is the most significant. This may be important, as some stents which may be able to withstand compression may fracture under bending, and vice versa. Selection of an appropriate stent according to location may help improve clinical success rates, although analysis of specific stent designs under specific loading conditions are required to confirm this.

Stent strut thickness was predicted to be an important factor in-stent performance for the design investigated in

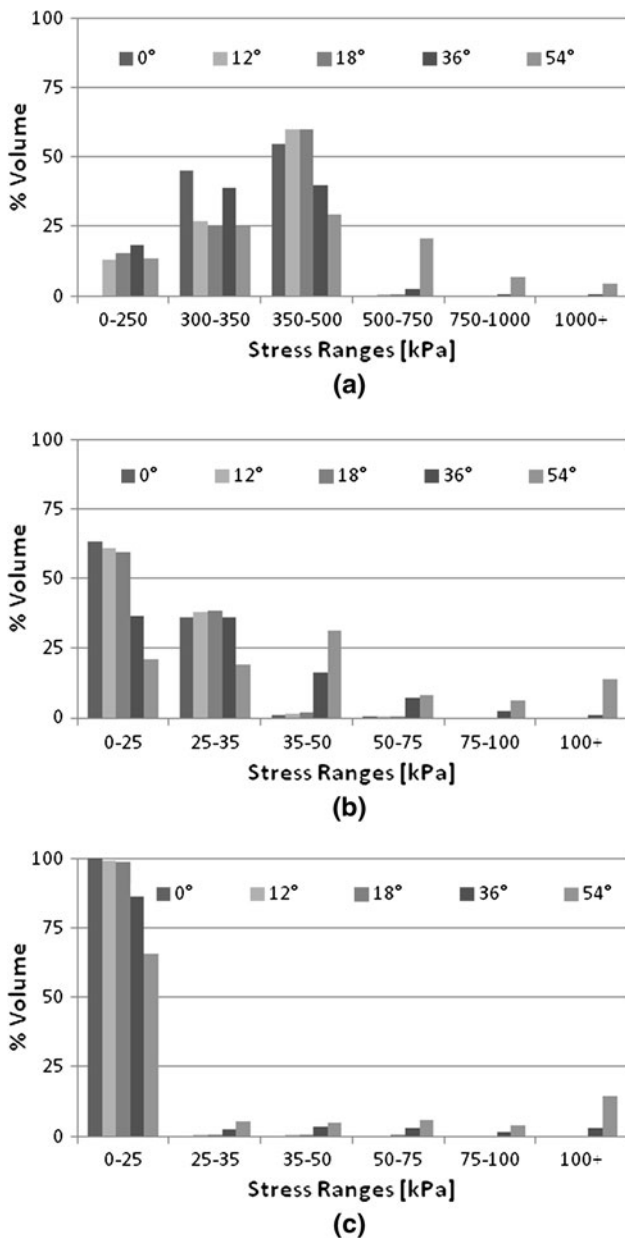


**Fig. 6** Stress distributions in **a** intima, **b** media and **c** adventitia at various stages of bending following insertion of SES (thickness = 150  $\mu\text{m}$ )

this study. Increasing the strut thickness was predicted to cause an increase in arterial stresses following stent deployment and following arterial bending relative to thinner struts. However, this increase in stress was predicted to be small in all layers of the artery. Stents with thicker struts also produced lower strain amplitudes during bending, decreasing the likelihood of fatigue failure. At low magnitudes of compression, thinner struts were predicted to produce superior fatigue results. There is, therefore, a trade-off between reducing stresses in the artery and improving fatigue performance in either bending or

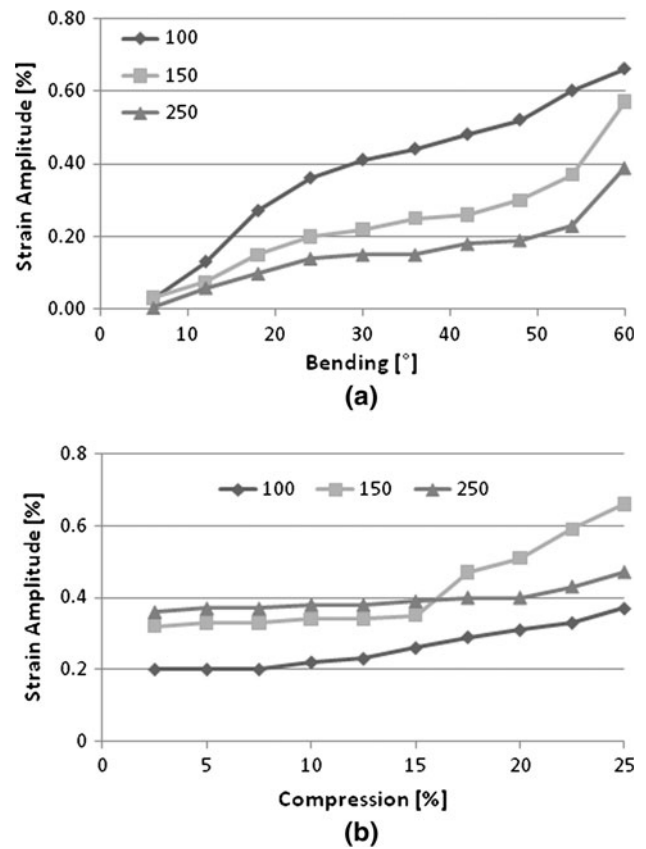


**Fig. 7 a** Predicted maximum stent strain amplitude following bending for SES with thicknesses of 100, 150 and 250  $\mu\text{m}$ . **b** Predicted maximum stent strain amplitude following compression for SES with thicknesses of 100, 150 and 250  $\mu\text{m}$

compression. In the case of bending, it can be argued that the increase in arterial stresses associated with stents with thicker struts is small relative to the benefit of improved fatigue behaviour. For example, the SES with a strut thickness of 250  $\mu\text{m}$  was predicted not to fail in fatigue with a maximum strain amplitude below 0.4%, and produced a relatively small increase in arterial stress. A further advantage of increasing the strut thickness of SES is that it was predicted to lead to an increase in lumen gain. Such an approach may be more preferable to oversizing of a SES, which also plays a key role in determining neointimal proliferation [37] and is predicted to increase the risk of fatigue failure (data not shown). Of course, there are numerous other stent design changes that will alter the functional characteristics of the stent. These include factors such as the spacing of struts and the shape of the stent cell. It has been demonstrated that for the same strut thickness, different compliances can be achieved by utilizing such design changes [3]. Given the role that altered strut thickness is predicted to have on device functionality, future studies need to also consider these design variables. The finite element method used here would be a suitable

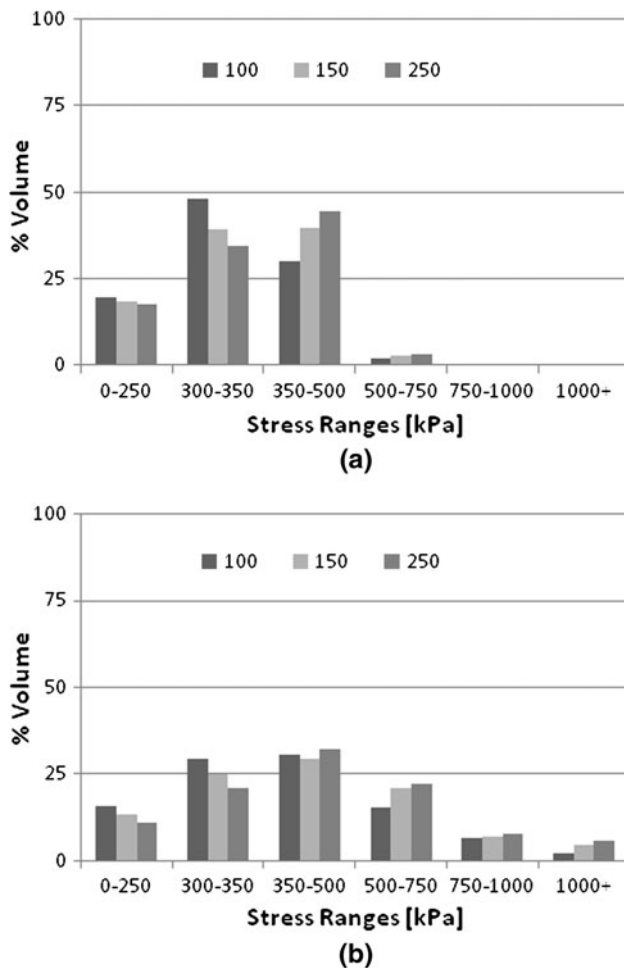


**Fig. 8** Stress distributions in intima of artery following deployment of SES with thicknesses of 100, 150 and 250  $\mu\text{m}$  after bending of **a** 36° and **b** 54°

tool for such assessing such design modifications, while physical testing like that performed elsewhere would be an appropriate method for validation [23]. In one of the few lesion sites that drug elution has not significantly improved results [8], improving the mechanical design and behaviour of the stent is essential towards making stenting a viable treatment for PAD.

The maximum bending and compression values of 60° and 25%, respectively applied to the arteries is in the upper end of that measured in human cadaver studies [23]. In that study, the bending value used for testing for fracture was 48°, with a value of 5% taken for compression. Therefore, the higher values of bending and compression applied in this study may over-estimate the bending and compression normally experienced *in vivo*. However, by measuring values for different increments of compression and bending (e.g. every 6° of bending), a more complete picture has been built up. Other limitations of the study include the use of cylindrical, isotropic, elastic, and non-diseased arteries. Using an isotropic, elastic material model will not give a fully accurate prediction of the artery stresses, but is reasonably valid for a comparative study such as this. In the absence of comprehensive layer specific data in the literature, the material properties of the iliac artery are used for all simulations. In reality, material properties will change continuously between the iliac and popliteal arteries. While all of these assumptions will influence the predicted magnitudes of stress and strain in both tissue and stent, we do not believe the overriding findings of the study (in terms of the influence of arterial bending and compression on BES and SES stenting) would change if these limitations were addressed. Further, the assumption of symmetry may not be fully valid, though it does represent the bench-top testing used in industry and published elsewhere [23]. The FE simulation did not consider crimping of the BES, which may influence the opening characteristics of the stent. Bending and compression boundary conditions were applied individually, but in reality they are coupled. Applying such complex boundary conditions to contacting bodies (stent–artery) has proven challenging, but should become possible with further increases in computational power. Another limitation of the study is the assumption of friction free contact, which will influence the magnitude of predicted arterial and stent stresses. Such analysis is further complicated by the fact that stents are rapidly covered by neotissue following implantation, thereby incorporating the stent into the artery wall. Further studies are required to investigate how neointimal tissue formation around the

**Table 1** Summary of maximum strain amplitudes (and minimum factors of safety) for pulsatile, bending and compression loading of peripheral arteries after knee/hip flexion of 70°/20°

	Bending/compression values	Pulsatile FOS <sup>a</sup>	Bending FOS	Compression FOS	Lowest FOS
Iliac	–	8.89	–	–	8.89 (Pulsatile)
Femoral	3°/5%	8.89	26.67	2.42	2.42 (Compression)
Femoro-popliteal	11°/14%	8.89	5.56	2.31	2.31 (Compression)
Popliteal	33°/9%	8.89	1.70	2.38	1.70 (Bending)

<sup>a</sup> Pulsatile values taken from [10]



implant will influence stent stresses due to vessel bending and compression. Finally we assumed only a single artery diameter in this study, whereas in reality the diameter will vary along the length of the vascular tree. Regardless, we do not believe that the overriding conclusions of the study would be influenced by these limitations.

In conclusion, the results presented in this study demonstrate the contribution of artery bending and compression towards increased tissues stresses in stented arteries, and the deformation and fatigue of the stents. The hypothesis of the study, that the mechanical environment produced by joint flexion raises arterial stresses and can potentially lead to stent fatigue, is corroborated for the specific BES and SES designs investigated here. To increase fatigue life and reduce arterial injury, location specific stent designs are required for peripheral arteries.

**Acknowledgment** This project was funded in part by a grant from Enterprise Ireland (CFTD/07/129).

## References

- Auricchio F, Petrini L (2002) Improvements and algorithmical considerations on a recent three-dimensional model describing stress-induced solid phase transformations. *Int J Numer Methods Eng* 55(11):1255–1284
- Ballyk PD (2006) Intramural stress increases exponentially with stent diameter: a stress threshold for neointimal hyperplasia. *J Vasc Interv Radiol* 17(7):1139–1145
- Bedoya J, Meyer CA, Timmins LH et al (2006) Effects of stent design parameters on normal artery wall mechanics. *J Biomech Eng* 128(5):757–765
- Boyle CJ, Lennon AB, Early M et al (2010) Computational simulation methodologies for mechanobiological modelling: a cell-centred approach to neointima development in stents. *Philos Trans R Soc A* 368(1921):2919–2935
- Capelli C, Gervaso F, Petrini L et al (2009) Assessment of tissue prolapse after balloon-expandable stenting: influence of stent cell geometry. *Med Eng Phys* 31(4):441–447
- Cejna M, Thurnher S, Illiasch H et al (2001) PTA versus Palmaz stent placement in femoropopliteal artery obstructions: a multicenter prospective randomized study. *J Vasc Interv Radiol* 12(1):23–31
- Cheng CP, Wilson NM, Hallett RL et al (2006) In vivo MR angiographic quantification of axial and twisting deformations of the superficial femoral artery resulting from maximum hip and knee flexion. *J Vasc Interv Radiol* 17(6):979–987
- Duda SH, Bosiers M, Lammer J et al (2005) Sirolimus-eluting versus bare nitinol stent for obstructive superficial femoral artery disease: the SIROCCO II trial. *J Vasc Interv Radiol* 16(3):331–338
- Duda SH, Bosiers M, Lammer J et al (2006) Drug-eluting and bare nitinol stents for the treatment of atherosclerotic lesions in the superficial femoral artery: long-term results from the SIROCCO trial. *J Endovasc Ther* 13(6):701–710
- Early M, Kelly DJ (2010) The role of vessel geometry and material properties on the mechanics of stenting in the coronary and peripheral arteries. *Proc Inst Mech Eng H* 224(3):465–476
- Early M, Lally C, Prendergast PJ et al (2009) Stresses in peripheral arteries following stent placement: a finite element analysis. *Comput Methods Biomech Biomed Eng* 12(1):25–33
- Favier D, Liu Y, Orgeas L et al (2006) Influence of thermomechanical processing on the superelastic properties of a Ni-rich nitinol shape memory alloy. *Mater Sci Eng A* 429(1–2):130–136
- Gervaso F, Capelli C, Petrini L et al (2008) On the effects of different strategies in modelling balloon-expandable stenting by means of finite element method. *J Biomech* 41(6):1206–1212
- Holzappel GA, Stadler M, Gasser TC (2005) Changes in the mechanical environment of stenotic arteries during interaction with stents: computational assessment of parametric stent designs. *J Biomech Eng* 127(1):166–180
- Holzappel GA, Schulze-Bauer CAJ, Stadler M (2000) Mechanics of angioplasty: wall, balloon and stent. In: Casey J, Bao G (eds) *Mechanics in Biology* ASME, New York
- Hsiao HM, Nikanorov A, Prabhu S et al (2007) Simulation of renal stent in respiration. In: *Proceedings of the frontiers in biomedical devices conference*, Irvine
- Jaff M (2004) The nature of SFA disease. *Endovasc Today* 4:13–15
- Lally C, Dolan F, Prendergast PJ (2005) Cardiovascular stent design and vessel stresses: a finite element analysis. *J Biomech* 38(8):1574–1581
- Menichelli M, Parma A, Pucci E et al (2007) Randomized trial of sirolimus-eluting stent versus bare-metal stent in acute myocardial infarction (SESAMI). *J Am Coll Cardiol* 49(19):1924–1930
- Migliavacca F, Petrini L, Massarotti P et al (2004) Stainless and shape memory alloy coronary stents: a computational study on the interaction with the vascular wall. *Biomech Model Mechanobiol* 2(4):205–217
- Mortier P, De Beule M, Van Loo D et al (2009) Finite element analysis of side branch access during bifurcation stenting. *Med Eng Phys* 31(4):434–440
- Mortier P, Holzappel GA, De Beule M et al (2010) A novel simulation strategy for stent insertion and deployment in curved coronary bifurcations: comparison of three drug-eluting stents. *Ann Biomed Eng* 38(1):88–99
- Nikanorov A, Smouse HB, Osman K et al (2008) Fracture of self-expanding nitinol stents stressed in vitro under simulated intravascular conditions. *J Vasc Surg* 48(2):435–440
- Pelton AR, Schroeder V, Mitchell MR et al (2008) Fatigue and durability of nitinol stents. *J Mech Behav Biomed Mater* 1(2):153–164
- Pericevic I, Lally C, Toner D et al (2009) The influence of plaque composition on underlying arterial wall stress during stent expansion: the case for lesion-specific stents. *Med Eng Phys* 31(4):428–433
- Prendergast PJ, Lally C, Daly S et al (2003) Analysis of prolapse in cardiovascular stents: a constitutive equation for vascular tissue and finite-element modelling. *J Biomech Eng* 125(5):692–699
- Scheinert D, Scheinert S, Sax J et al (2005) Prevalence and clinical impact of stent fractures after femoropopliteal stenting. *J Am Coll Cardiol* 45(2):312–315
- Schievano S, Taylor AM, Capelli C et al (2010) Patient specific finite element analysis results in more accurate prediction of stent fractures: application to percutaneous pulmonary valve implantation. *J Biomech* 43(4):687–693
- Schillinger M, Sabeti S, Loewe C et al (2006) Balloon angioplasty versus implantation of nitinol stents in the superficial femoral artery. *N Engl J Med* 354(18):1879–1888
- Schulze-Bauer CA, Morth C, Holzappel GA (2003) Passive biaxial mechanical response of aged human iliac arteries. *J Biomech Eng* 125(3):395–406

31. Smouse HB, Nikanorov A, LaFlash D (2005) Biomechanical forces in the femoropopliteal arterial segment. *Endovasc Today* 4:60–66
32. Timmins LH, Meyer CA, Moreno MR et al (2008) Effects of stent design and atherosclerotic plaque composition on arterial wall biomechanics. *J Endovasc Ther* 15(6):643–654
33. Wiersma S, Dolan F, Taylor D (2006) Fatigue and fracture in materials used for micro-scale biomedical components. *Biomed Mater Eng* 16(2):137–146
34. Wu W, Wang WQ, Yang DZ et al (2007) Stent expansion in curved vessel and their interactions: a finite element analysis. *J Biomech* 40(11):2580–2585
35. Wu W, Qi M, Liu XP et al (2007) Delivery and release of nitinol stent in carotid artery and their interactions: a finite element analysis. *J Biomech* 40(13):3034–3040
36. Zahedmanesh H, John Kelly D, Lally C (2010) Simulation of a balloon expandable stent in a realistic coronary artery—determination of the optimum modelling strategy. *J Biomech* 43(11): 2126–2132
37. Zhao HQ, Nikanorov A, Virmani R et al (2009) Late stent expansion and neointimal proliferation of oversized Nitinol stents in peripheral arteries. *Cardiovasc Intervent Radiol* 32(4):720–726